Published in final edited form as:
J Neural Eng. 2011 August ; 8(4): 046007. doi:10.1088/1741-2560/8/4/046007.

Simultaneous recording of rat auditory cortex and thalamus via a titanium-based, microfabricated, microelectrode device

PT McCarthy[1], **MP Rao**[2], and **KJ Otto**[3]

[1]Department of Mechanical Engineering, Purdue University, West Lafayette, IN 47907

[2]Department of Mechanical Engineering, University of California-Riverside, Riverside, CA 92521

[3]Departments of Biological Sciences and the Weldon School of Biomedical Engineering, Purdue University, West Lafayette, IN 47907

Abstract

Direct recording from sequential processing stations within the brain has provided opportunity for enhancing understanding of important neural circuits, such as the corticothalamic loops underlying auditory, visual, and somatosensory processing. However, the common reliance upon microwire-based electrodes to perform such recordings often necessitates complex surgeries and increases trauma to neural tissues. This paper reports the development of titanium-based, microfabricated, microelectrode devices designed to address these limitations by allowing acute recording from the thalamic nuclei and associated cortical sites simultaneously in a minimally-invasive manner. In particular, devices were designed to simultaneously probe rat auditory cortex and auditory thalamus, with the intent of recording auditory response latencies and isolated action potentials within the separate anatomical sites. Details regarding the design, fabrication, and characterization of these devices are presented, as are preliminary results from acute *in vivo* recording.

1. Introduction

By providing capability for direct recording from discrete neurons and neuron ensembles, penetrating microelectrodes have aided the field of neuroscience in elucidating the mechanisms by which information is processed in the brain (1, 2). Microfabrication technologies derived from integrated circuit manufacturing have greatly advanced these efforts by enabling realization of microelectrode devices with improved recording consistency and yield, as well as higher recording site density and spatial positioning accuracy relative to microwire based electrodes (3-6). Thus far, microfabricated microelectrodes have typically employed either the “Michigan” or “Utah” architectures (7, 8), the former consisting of planar penetrating shanks with a multiplicity of recording sites along their length, and the latter consisting of three-dimensional arrays of penetrating shanks with single, tip-located recording sites. Three-dimensional Michigan type devices have also been demonstrated by assembling stacks of planar arrays (9-12), thus allowing high density recordings at multiple depths within the volume being probed.

Although microfabricated microelectrodes are typically designed for cortical recording, capability for simultaneous cortical and thalamic recording is also of interest. This interest is driven by the desire to probe the complexity of the corticothalamic loop (13-15), which consists of ascending, descending, and recurrent sets of neuronal connections (16). While simultaneous corticothalamic recording has been reported by others, these efforts have relied

Contact: Kevin J. Otto, kotto@purdue.edu.

on use of microwire-based microelectrodes (17-19). Since each microwire only provides capability for single-site recording, studies of large numbers of discrete neurons or neuronal ensembles requires use of correspondingly large numbers of devices, which increases surgical complexity, as well as trauma to the brain. Microfabricated microelectrodes would provide capability for high-density recordings in multiple anatomical sites along their insertion pathways in a less invasive manner, thus providing impetus for their development.

Recently, we reported the realization of titanium-based devices designed to address this need, which enabled the first demonstration of simultaneous acute corticothalamic recording using a single microfabricated penetrating microelectrode (20). Titanium represents a new material for microfabricated microelectrodes whose use is motivated by the desire to mitigate limitations associated with prevailing device materials (21, 22), such as the intrinsic brittleness of silicon and the poor rigidity of polymeric materials. Herein, we expand upon this report to detail the design, fabrication, and testing of these devices *in vitro* and *in vivo*.

2. Methods

2.1. Device design, fabrication, and packaging

Devices with shank lengths of 4.9 & 5.4 mm were designed for acute recording in the auditory cortex and thalamus of the rat model. Both device types were modeled on commercially-available "Michigan" type microelectrode arrays (*e.g.* A1 × 16 − 5 mm 100 - 413, NeuroNexus Technologies, Ann Arbor, MI; Shank Length − 5 mm, Recording Site Diameter − 23 μm, Recording Site Pitch − 100 μm). Each microelectrode device contained 16 independently addressable circular recording sites. Twelve distinct design variants were developed with different shank lengths (4.9, & 5.4 mm), recording site diameters (23 & 40 μm), and pitch (50, 100, & 150 μm) (21, 22). The given variation of the recording site diameter and pitch was reflective of the desire to eventually optimize the design parameters to develop the most consistent sampling of discrete neurons with high signal to noise ratio.

The microelectrodes were designed with two sets of recording sites, with the first set of eight sites positioned within 2 mm of the base of the microelectrode, and the second set either 2.9 or 3.4 mm further down the shaft. The exact positioning of the recording sites was determined by their diameter and pitch. This device design was chosen to maximize the number of sites monitoring electrophysiology in both the auditory cortex and thalamus. Figure 1 shows a schematic of a 4.9 mm microelectrode with thickness of 35 μm and width tapering from 65 – 209 μm.

The microelectrode fabrication process has been previously detailed elsewhere (21, 22). Briefly, titanium foil substrates with lateral dimensions of 25 mm × 25 mm and thickness of 25 ± 7.62 μm were cleaned in solvents, followed by deposition of SiO_x dielectric layer (0.6 μm) using plasma enhanced chemical vapor deposition (PECVD). A gold layer (0.5 μm) was then patterned using photolithographic lift-off techniques and electron-beam deposition. An additional dielectric layer was then deposited using a combination of Si_xN_y (0.2 μm) and SiO_x (0.8 μm). After the contact windows were opened using dry etching techniques, a mask layer consisting of Si_xN_y (0.2 μm) and SiO_x (3.0 μm) was deposited and patterned to form the microelectrode shank outline. Titanium inductively coupled plasma deep etch (TIDE) (23) was then performed to form the microelectrode, followed by a short dry etch of the dielectrics in order to reopen the contact windows. Figure 2 shows a cross-sectional schematic of a single trace fabricated within the microelectrode, while figure 3 shows scanning electron micrographs of the resulting titanium-based microelectrodes.

The microelectrode devices were packaged by bonding to commercially-available printed circuit boards (PCBs) (A-16, NeuroNexus Technologies) using cyanoacrylate adhesive.

Gold wire-bonding was then used to make connections between the contact pads on the devices and their respective bond pads on the PCBs (7400A, West-Bond, Anaheim, CA). Afterwards, an additional layer of cyanoacrylate was applied over the contact pad area as an encapsulant to protect the exposed wires. Figure 4 shows a titanium microelectrode bonded to a PCB with its contact pads wire-bonded to the PCB gold traces.

2.2. *In vitro* recording site cleaning

As described in greater detail elsewhere (22), devices were subjected to a 1 min, 1.5 V DC pulse using the *in vitro* EIS/CV testing apparatus described in Section 2.3. The resulting electrolysis at the recording sites facilitated removal of fabrication process residues, thus reducing impedance. This *in vitro* recording site cleaning process is similar to those that have been performed during *in vivo* studies with a shorter pulse duration (24, 25).

2.3. *In vitro* electrical testing

Electrochemical impedance spectroscopy (EIS) and cyclic voltammetry (CV) measurements were collected using an Autolab potentiostat PGSTAT12 (EcoChemie, Utrecht, The Netherlands) with built-in frequency analyzer (Brinkmann, Westbury, NY) (26). *In vitro* testing was performed utilizing a three-electrode setup. A calomel electrode (Fisher Scientific, Waltham, MA) was used as the reference electrode with a platinum wire as the counter electrode. As illustrated in figure 5, the microelectrode devices were immersed at room temperature in 1× phosphate-buffered saline (PBS) at sufficient depth to allow testing of all recording sites on the device. Measurements of recording sites were taken individually with the test apparatus isolated in a copper mesh “Faraday” cage (not shown in figure). A 25 mV RMA sine wave was applied to the recording site for EIS tests with frequencies ranging logarithmically from 0.1 to 10 kHz. CV testing was performed using a linear voltage sweep from -0.3 V to 0.8 V with a scanning rate of 1 V/s. This data was then used to calculate the charge carrying capacity as the area of the cathodal current within the potential limits of hydrolysis.

2.4. *In vivo* acute corticothalamic recording

In vivo electrical testing was performed in a rat model with the titanium microelectrodes. The goal of the testing was to examine the response to auditory stimulus within the auditory cortex and thalamus simultaneously. Two Long-Evans rats (Harlan, Indianapolis, IN) were chosen for testing. The rats were weighed and placed under anesthesia using a combination of ketamine hydrochloride (80 ml/kg body wt) and xylazine (5 ml/kg) with subsequent 1 mL injections of ketamine every 30 min as required to maintain an areflexic state. The experimental procedures complied with the guidelines for the care and use of laboratory animals and were approved by the Purdue Animal Care and Use Committee.

During surgery, a midline incision was made through the scalp and the muscles were retracted. Four holes were then drilled into the skull using a burr. Allen type screws were attached and a hexagonal nut was placed in the center as shown in figure 6. Dental acrylic (Co-Oral-Ite Dental Mfg. Co. Inc., Diamond Springs, CA) was placed over the screws and around the nut and left to dry creating a mold. Once the mold hardened, a head holder was attached to the hexagonal nut anterior to bregma. This mount served to stabilize the rat's skull during subsequent microelectrode insertion and testing. The skull over the primary auditory cortex of the right hemisphere was drilled open using a burr. Once the brain was exposed, the area was cleaned and prepared for device insertion.

Prior to insertion, cortical tonotopy was verified based on vascular landmarks (27). Based on stereotactic measurements (28), the devices were then inserted such that the 8 recording sites at the tip of the microelectrodes would interface with the auditory thalamus while the 8 sites

at the base of the microelectrodes would interface with the auditory cortex. The microelectrode devices were inserted through the intact dura mater into the cortical mantle. Broadband acoustic noise stimuli (70 dbSPL for 100 ms) were then administered via an external speaker approximately 10 cm from the animal's left pinna (RX7, Tucker-Davis Technologies (TDT), Alachua, FL). Recording was performed through the connection of an external pre-amplifier (MS16, TDT) connected to the microelectrode PCB. The pre-amplifier digitized and transmitted the neural signals to the RX7 neural recording system for amplification, analysis, and storage. Auditory physiological data were analyzed using custom software (MATLAB, Natick, MA) by constructing peri-stimulus time histograms of acoustic-noise evoked responses to verify electrode function and placement. The neural data analysis was conducted as per Ludwig *et al.* (29). Briefly, signals were first identified with custom-written MATLAB software based on peaks that were 3.5 standard deviations above and below the sample distribution. Subsequently, 2.4 ms snippets centered on the minimum of the peaks were removed from the recordings, and then the root mean squared amplitude of the remaining data was used as an estimate of the noise. The signal amplitude was calculated as the mean peak-to-peak amplitude of the originally removed snippets. Finally, the signal to noise ratio was calculated as the signal amplitude divided by 2× the noise amplitude.

3. Results

3.1. *In vitro* electrical testing

The EIS results for the titanium-based microelectrodes indicated impedance values between 0.20 – 0.43 MΩ at a frequency of 1 kHz for recording site diameters of 40 μm, while a range of 0.75 – 1.38 MΩ was found for smaller 23 μm recording sites (21, 22). CV tests revealed maximum charge carrying capacities ranging from 0.1 to 1.9 mC/cm^2. Figure 7 displays the resulting plots for a typical recording site. Commercially-available silicon microelectrodes typically have an impedance range of 0.5 – 3.0 MΩ at 1 kHz depending on the recording site diameter (NeuroNexus Technologies). Therefore, most of the impedance values for the titanium-based devices are comparable to these commercially-available devices. Also, current literature suggests that the charge carrying capacities of the gold recording sites are comparable (30).

3.2. *In vivo* acute corticothalamic recording

Two microelectrodes were successfully implanted: (Device #1) 4.9 mm length, 40 μm diameter sites, 100 μm recording site pitch, implanted into Rat #1; and (Device #2) 5.4 mm length, 23 μm diameter sites, 100 μm recording site pitch, implanted into Rat #2. Despite their significant length, the microelectrodes were able to penetrate the dura matter, whereas commercially-available silicon-based devices typically require retraction of the dura prior to insertion. While this demonstrates opportunity for simplification of surgical procedure afforded by use of titanium microelectrodes, it is important to acknowledge that this advantage arises primarily from the increased cross-sectional area of the titanium microelectrodes relative to first-generation, commercially-available, silicon-based microelectrodes (i.e. shank thicknesses of ~35 μm and ~15 μm, respectively). Si-based devices with greater cross-sectional areas are now available, and it is reasonable to expect that such devices might also provide sufficient stiffness for dural penetration. Figure 8 shows a sequence of images from the successful insertion of Device #1 through the dura matter. No buckling of this device was observed during its insertion. Slight buckling of Device #2 was observed during its insertion, but was quickly resolved once the dura was penetrated.

To verify the placement and functionality of the microelectrodes, broadband, acoustic noise stimuli were used to induce multi-channel responses via the same method presented in Section 2.4. Properly inserted and functioning microelectrodes would be expected to provide data of differing auditory response latencies for the two anatomical sites within the brain, with approximately a 15 ms delay in the auditory thalamus and approximately a 20 ms delay in the cortex from the onset of the stimulus, reflecting the acoustic transmission and neural processing delays. Although recordings of acoustic-evoked responses were achieved with both devices, the lack of thalamic latencies observed in Device #1 (data not shown) suggested that its length was insufficient to reach desired thalamic nuclei.

Figure 9 shows recording traces from Device #2, where normal acoustic threshold physiology was observed on 15 of the 16 recording sites and a number of clearly isolated action potentials were evident across several channels. Simultaneous recording from both cortex and thalamus was confirmed by the observation of expected auditory processing delays. Table 1 provides a summary of signal to noise ratio analyses of the recorded responses. The average signal to noise ratio of the 15 recording traces in this experiment was 5.23, which is comparable to “good” recordings from commercially-available microelectrode arrays (31). Figure 10 shows peri-stimulus time histograms generated by analyzing the auditory physiological data elicited by acoustic–noise bursts. Each box reflects the response from a single recording site. The top two rows reflect data from the 8 recording sites in the auditory cortex, while the bottom two rows reflect data from the 8 sites in the auditory thalamus. The horizontal axis within each image represents time from 20 ms before the acoustic noise burst to 300 ms afterwards. The vertical axis within each image reflects increasing intensity noise bursts (-100, 30, 40, 50, 60, 79 dB sound pressure levels). The expected auditory processing delays are evident and additional physiological phenomena (*i.e.* inhibition, offset-response) are also observed on some of the recording sites (*e.g.* Site 12 in figure 10). Significantly more inhibition and offset responses are observed in auditory cortex (the top two rows of figure 10). Furthermore, one thalamic site (site 14, figure 10) exhibited a sustained response to the acoustic stimulus.

4. Discussion

The simultaneous recording of auditory thalamus and cortex is of interest to neuroscientists and neuroengineers attempting to reverse-engineer the brain via the corticothalamic loop. Nicolelis *et al.* have reported several studies recording in multiple cortical and sub-cortical structures within the somatosensory system simultaneously (17-19). In these studies, recordings of up to 135 neurons in multiple anatomical sites were performed simultaneously using up to three electrode arrays, each containing 8-16 microwires (50 μm diameter). While these studies offered unprecedented insight into communication and function within the somatosensory system, this came at the expense of extensive damage to the neural tissue. Since a single microfabricated titanium microelectrode device provides opportunity for simultaneous recording from multiple anatomical sites along its insertion pathway, the number of device insertions required for such studies can be reduced, thus, significantly reducing surgical complexity and trauma. Moreover, reduced trauma would also provide potential for greater long-term recording reliability in chronic studies, since studies have suggested that the latter is strongly influenced by the former (32, 33). Finally, we expect that the current device design could be easily modified to accommodate visual or somatosensory corticothalamic loop studies as well, thus further broadening its potential utility.

The data presented herein expand upon our earlier reporting of the first simultaneous corticothalamic recording using a single titanium-based microfabricated microelectrode (20). However, it is important to acknowledge a recent report by Torfs *et al.* demonstrating similar capability using silicon-based microelectrodes (34). In this report, which was an

extension of earlier efforts based on similar devices (9, 35), two-dimensional Michigan-style microelectrodes were demonstrated. A unique feature of these devices was the monolithic integration of switching electronics, which provided capability for simultaneous recording from eight independent recording sites selectable from 256 total sites available on the device. This enabled real-time selection of recording sites to optimize recording quality and/or selectively target neural regions of interest, such as the cortex and thalamus.

The fabrication of the titanium-based devices presented herein was made possible by recently-developed techniques that allow, for the first time, deep etching of bulk titanium substrates (23, 36). As demonstrated in our earlier studies (22), titanium possesses a number of advantageous properties that make it a desirable structural material for microelectrodes. For example, its fracture toughness, which is a measure of resistance to crack propagation, far exceeds that of silicon ($55\ \text{MPa}\sqrt{\text{m}}$ and $0.95\ \text{MPa}\sqrt{\text{m}}$ (37), for Ti and Si, respectively), thus enhancing safety by minimizing potential for device fragmentation within the brain. Moreover, its elastic modulus, which is a measure of the effective “stiffness” of the material, far exceeds that of polymeric materials (107 GPa (37) and 4 GPa (38), for Ti and polyimide, respectively), thus allowing for reduction of device cross section, without adversely affecting insertion reliability and placement accuracy. Finally, its intrinsic capability to plastically deform allows for retention of recording functionality under loading situations that would cause comparable silicon-based devices to fracture and lose all functionality.

Despite these advantageous properties, it is important to also acknowledge the potential limitations imposed by the use of titanium. For example, monolithic integration of electrical switching capability similar to that demonstrated by Torfs *et al.* is precluded, since this requires use of a semiconducting material, such as silicon. Moreover, it is conceivable that the electrical conductivity of titanium might allow shorting between neurons contacting the exposed underside of the device. Although evidence of such shorting was not observed in the current study, this issue could be easily mitigated by coating of the exposed titanium with insulating materials (e.g. SiO_2, Si_3N_4, or polyimide). Finally, as with silicon-based devices, large elastic modulus mismatch with surrounding neural tissue (166 GPa (38), 107 GPa (37), and 1-10 GPa (39), for Si, Ti, & brain, respectively] may result in generation of micromotion-induced inflammation that could degrade recording quality in chronically-implanted devices (40, 41).

Finally, it is important to acknowledge that chronic implantation studies are still needed to assess long-term stability and recording reliability of the titanium-based microelectrode devices. For example, vascular damage is a concern for any penetrating device, thus techniques to avoid vascular penetration or minimize subsequent inflammation would likely increase reliability (42-44). Moreover, while the intrinsic toughness of titanium will enhance mechanical reliability, use of titanium in and of itself is unlikely to mitigate potential for a reactive tissue response (*i.e.* gliosis), since there will still be a foreign body response (45-47). Various strategies to limit the reactive tissue response have been previously explored, including pharmacological intervention (43, 48-52), surface modification (53, 54), and novel device design (33, 55). Future studies will focus on establishing the chronic recording reliability of titanium-based microelectrodes and exploring opportunities for implementation of such strategies. In addition, future studies will seek to exploit the opportunity provided by these devices to study corticothalamic communication and function by stimulating within one anatomical site while recording in the other, all in a minimally-invasive manner.

5. Conclusion

We have reported the design, fabrication, and *in vitro* and acute *in vivo* testing of titanium-based, microfabricated, microelectrodes for simultaneous corticothalamic recording in rat. *In vitro* characterization studies demonstrate that the devices provide recording performance comparable to that of commercially-available silicon-based devices. Results from *in vivo* studies demonstrate simultaneous recording of multi-unit data and isolated action potentials in rat auditory cortex and thalamus. These results demonstrate the potential embodied within such devices to serve as an enabling tool for neurophysiological studies focused on elucidating the mechanisms underlying corticothalamic communication.

Acknowledgments

The authors would like to thank the Center for Neural Communication Technology for providing the silicon microelectrode arrays (NIH/NIBIB P41-EB002030). The authors would also like to thank the staff at the Birck Nanotechnology Center (Purdue University), and the students of the NeuroProstheses Research Laboratory (Purdue University Weldon School of Biomedical Engineering). The work was supported by a Cordier Fellowship, the Purdue Research Foundation, and Showalter Research Trust, Purdue University.

References

1. Kruger J. Simultaneous individual recordings from many cerebral neurons: techniques and results. Rev Physiol Biochem Pharmacol. 1983; 98:177–233. [PubMed: 6361965]
2. Blum NA, Carkhuff BG, Charles HK, Edwards RL, Meyer RA. Multisite microprobes for neural recordings. IEEE Transactions on Biomedical Engineering. 1991; 38(1):68–74. [PubMed: 2026434]
3. Drake KL, Wise KD, Farraye J, Anderson DJ, BeMent SL. Performance of planar multisite microprobes in recording extracellular single-unit intracortical activity. IEEE Trans Biomed Eng. 1988 Sep; 35(9):719–32. [PubMed: 3169824]
4. Ensell G, Banks DJ, Ewins DJ, Balachandran W, Richards PR. Silicon-based microelectrodes for neurophysiology fabricated using a gold metallization/nitride passivation system. Journal of MicroElectroMechanical Systems. 1996 June; 5(2):117–21.
5. Yoon TH, Hwang EJ, Shin DY, Park SI, Oh SJ, Jung SC, et al. A micromachined silicon depth probe for multichannel neural recording. IEEE Trans Biomed Eng. 2000 Aug; 47(8):1082–7. [PubMed: 10943057]
6. Norlin, P.; Kindlundh, M.; Mouroux, A.; Yoshida, K.; Jensen, W.; Hofmann, UG., editors. A 32-site neural recording probe fabricated by double-sided deep reactive ion etching of silicon-on-insulator substrates. Micromechanics Europe Workshop; Cork, Ireland. 2001.
7. Campbell PK, Jones KE, Huber RJ, Horch KW, Normann RA. A silicon-based, three-dimensional neural interface: manufacturing processes for an intracortical electrode array. IEEE Transactions on Biomedical Engineering. 1991 Aug; 38(8):758–68. [PubMed: 1937509]
8. Najafi K, Wise KD, Mochizuki T. A high-yield IC-compatible multichannel recording array. Electron Devices, IEEE Transactions on. 1985; 32(7):1206–11.
9. Neves, HP.; Orban, GA.; Koudelka-Hep, M.; Stieglitz, T.; Ruther, P. Development of modular multifunctional probe arrays for cerebral applications. 2007 3rd International IEEE/EMBS Conference on Neural Engineering, Vols 1 and 2; 2007. p. 104-9.
10. Herwik S, Kisban S, Aarts AAA, Seidl K, Girardeau G, Benchenane K, et al. Fabrication technology for silicon-based microprobe arrays used in acute and sub-chronic neural recording. Journal of Micromechanics and Microengineering. 2009; 19(7)
11. Du JG, Roukes ML, Masmanidis SC. Dual-side and three-dimensional microelectrode arrays fabricated from ultra-thin silicon substrates. Journal of Micromechanics and Microengineering. 2009; 19(7)
12. Hoogerwerf AC, Wise KD. A three-dimensional microelectrode array for chronic neural recording. IEEE Transactions on Biomedical Engineering. 1994 Dec; 41(12):1136–46. [PubMed: 7851915]
13. Rouiller EM, Welker E. A comparative analysis of the morphology of corticothalamic projections in mammals. Brain Research Bulletin. 2000; 53(6):727–41. [PubMed: 11179837]

14. Hillenbrand U, van Hemmen JL. Adaptation in the corticothalamic loop: Computational prospects of tuning the senses. Philosophical Transactions of the Royal Society of London Series B-Biological Sciences. 2002; 357(1428):1859–67.
15. Briggs F, Usrey WM. Emerging views of corticothalamic function. Current Opinion in Neurobiology. 2008; 18(4):403–7. [PubMed: 18805486]
16. Alitto HJ, Usrey WM. Corticothalamic feedback and sensory processing. Current Opinion in Neurobiology. 2003; 13(4):440–5. [PubMed: 12965291]
17. Nicolelis MAL, Chapin JK. Spatiotemporal structure of somatosensory responses of many-neuron ensembles in the rat ventral posterior medial nucleus of the thalamus. Journal of Neuroscience. 1994; 14(6):3511–32. [PubMed: 8207469]
18. Nicolelis MAL, Ghazanfar AA, Faggin BM, Votaw S, Oliveira LMO. Reconstructing the engram: Simultaneous, multisite, many single neuron recordings. Neuron. 1997; 18(4):529–37. [PubMed: 9136763]
19. Faggin BM, Nguyen KT, Nicolelis MAL. Immediate and simultaneous sensory reorganization at cortical and subcortical levels of the somatosensory system. Proceedings of the National Academy of Sciences of the United States of America. 1997; 94(17):9428–33. [PubMed: 9256499]
20. McCarthy, PT.; Rao, MP.; Otto, KJ. Corticothalamic neural recording via penetrating titanium microelectrodes. Neural Interfaces Conference; June 21-23; Long Beach, CA. 2010. p. 77
21. McCarthy, PT.; Madangopal, R.; Otto, KJ.; Rao, MP. Titanium-based multi-channel, microelectrode array for recording neural signals. 31st Annual International Conference of the IEEE Engineering in Medicine and Biology Conference; Sept. 2-6, 2009; Minneapolis, Minnesota. 2009.
22. McCarthy P, Otto K, Rao M. Robust penetrating microelectrodes for neural interfaces realized by titanium micromachining. Biomedical Microdevices. 2011; 13(3):503–13. [PubMed: 21360044]
23. Parker ER, Thibeault BJ, Aimi MF, Rao MP, MacDonald NC. Inductively coupled plasma etching of bulk titanium for MEMS applications. Journal of the Electrochemical Society. 2005; 152(10):C675–C83.
24. Johnson MD, Otto KJ, Kipke DR. Repeated voltage biasing improves unit recordings by reducing resistive tissue impedances. IEEE Transactions on Neural Systems and Rehabilitation Engineering. 2005 Jun; 13(2):160–5. [PubMed: 16003894]
25. Otto KJ, Johnson MD, Kipke DR. Voltage pulses change neural interface properties and improve unit recordings with chronically implanted microelectrodes. IEEE Transactions on Biomedical Engineering. 2006; 53(2):333–40. [PubMed: 16485763]
26. Pierce AL, Sommakia S, Rickus JL, Otto KJ. Thin-film silica sol-gel coatings for neural microelectrodes. Journal of Neuroscience Methods. 2009
27. Sally SL, Kelly JB. Organization of auditory-cortex in the albino-rat-sound frequency. Journal of Neurophysiology. 1988; 59(5):1627–38. [PubMed: 3385476]
28. Paxinos G, Watson C. The rat brain in stereotaxic coordinates. Neuroscience Letters. 1981; (Suppl. (8)):S71.
29. Ludwig KA, Uram JD, Yang JY, Martin DC, Kipke DR. Chronic neural recordings using silicon microelectrode arrays electrochemically deposited with a poly(3,4-ethylenedioxythiophene) (PEDOT) film. Journal of Neural Engineering. 2006; 3(1):59–70. [PubMed: 16510943]
30. Wise KD, Anderson DJ, Hetke JF, Kipke DR, Najafi K. Wireless implantable microsystems: High-density electronic interfaces to the nervous system. Proceedings of the IEEE. 2004 Jan; 92(1):76–97.
31. Suner S, Fellows MR, Vargas-Irwin C, Nakata GK, Donoghue JP. Reliability of signals from a chronically implanted, silicon-based electrode array in non-human primate primary motor cortex. IEEE Transactions on Neural Systems and Rehabilitation Engineering. 2005; 13(4):524–41. [PubMed: 16425835]
32. Szarowski DH, Andersen MD, Retterer S, Spence AJ, Isaacson M, Craighead HG, et al. Brain responses to micro-machined silicon devices. Brain Research. 2003 Sep 5; 983(1-2):23–35. [PubMed: 12914963]
33. Seymour JP, Kipke DR. Neural probe design for reduced tissue encapsulation in CNS. Biomaterials. 2007 Sep; 28(25):3594–607. [PubMed: 17517431]

34. Torfs, T.; Ulbert, I.; Seidl, K. Two-dimensional multi-channel neural probes with electronic depth control. IEEE Biomedical Circuits and Systems Conference; Nov 3-5; Paphos, Cyprus. 2010. p. 198-201.
35. Seidl, K.; Herwik, S.; Nurcahyo, Y.; Torfs, T.; Keller, M.; Schuttler, M., et al. CMOS-based high-density silicon microprobe array for electronic depth control in neural recording. Micro Electro Mechanical Systems, 2009 MEMS 2009 IEEE 22nd International Conference on; 25-29 Jan 2009; p. 232-5.
36. Aimi MF, Rao MP, MacDonald NC, Zuruzi AS, Bothman DP. High-aspect-ratio bulk micromachining of titanium. Nature materials. 2004 Feb; 3(2):103–5.
37. Callister, WD. Materials science and engineering : An introduction. 6th. New York: Wiley; 2003.
38. Senturia, SD. Microsystem design. New York: Springer; 2004.
39. Lippert, SA.; Grimm, MJ. Estimating the material properties of brain tissue at impact frequencies: A curve-fitting solution. Summer Bioengineering Conference; June 25-29; Key Biscayne, Florida. 2003.
40. Muthuswamy, J.; Saha, R.; Gilletti, A. Tissue micromotion induced stress around brain implants. 2005 3rd IEEE/EMBS Special Topic Conference on Microtechnology in Medicine and Biology; 2005. p. 102-3.
41. Gilletti A, Muthuswamy J. Brain micromotion around implants in the rodent somatosensory cortex. Journal of Neural Engineering. 2006; 3(3):189–95. [PubMed: 16921202]
42. Bjornsson CS, Oh SJ, Al-Kofahi YA, Lim YJ, Smith KL, Turner JN, et al. Effects of insertion conditions on tissue strain and vascular damage during neuroprosthetic device insertion. Journal of Neural Engineering. 2006; 3(3):196–207. [PubMed: 16921203]
43. Shain W, Spataro L, Dilgen J, Haverstick K, Retterer S, Isaacson M, et al. Controlling cellular reactive responses around neural prosthetic devices using peripheral and local intervention strategies. IEEE Transactions on Neural Systems and Rehabilitation Engineering. 2003; 11(2): 186–8. [PubMed: 12899270]
44. Kozai TDY, Marzullo TC, Hooi F, Langhals NB, Majewska AK, Brown EB. Reduction of neurovascular damage resulting from microelectrode insertion into the cerebral cortex using in vivo two-photon mapping. Journal of Neural Engineering. 2010; 7(4, Sp. Iss. SI)
45. Williams JC, Rennaker RL, Kipke DR. Long-term neural recording characteristics of wire microelectrode arrays implanted in cerebral cortex. Brain Research Protocols. 1999; 4(3):303–13. [PubMed: 10592339]
46. Vetter RJ, Williams JC, Hetke JF, Nunamaker EA, Kipke DR. Chronic neural recording using silicon-substrate microelectrode arrays implanted in cerebral cortex. IEEE Transactions on Biomedical Engineering. 2004; 51(6):896–904. [PubMed: 15188856]
47. Williams JC, Hippensteel JA, Dilgen J, Shain W, Kipke DR. Complex impedance spectroscopy for monitoring tissue responses to inserted neural implants. Journal of Neural Engineering. 2007; 4(4): 410–23. [PubMed: 18057508]
48. Zhong, Y.; McConnell, GC.; Ross, JD.; DeWeerth, SP.; Bellamkonda, RV. A novel dexamethasone-releasing, anti-inflammatory coating for neural implants. 2005 2nd Internatinoal IEEE/EMBS Conference on Neural Engineering; 2005. p. 522-5.
49. Kim DH, Martin DC. Sustained release of dexamethasone from hydrophilic matrices using PLGA nanoparticles for neural drug delivery. Biomaterials. 2006 May; 27(15):3031–7. [PubMed: 16443270]
50. Wadhwa R, Lagenaur CF, Cui XT. Electrochemically controlled release of dexamethasone from conducting polymer polypyrrole coated electrode. Journal of Controlled Release. 2006; 110(3): 531–41. [PubMed: 16360955]
51. Zhong YH, Bellamkonda RV. Dexamethasone-coated neural probes elicit attenuated inflammatory response and neuronal loss compared to uncoated neural probes. Brain Research. 2007; 1148:15–27. [PubMed: 17376408]
52. Grand L, Wittner L, Herwik S, Gothelid E, Ruther P, Oscarsson S, et al. Short and long term biocompatibility of NeuroProbes silicon probes. Journal of Neuroscience Methods. 2010; 189(2): 216–29. [PubMed: 20399227]

53. Moxon KA, Kalkhoran NM, Markert M, Sambito MA, McKenzie JL, Webster JT. Nanostructured surface modification of ceramic-based microelectrodes to enhance biocompatibility for a direct brain-machine interface. IEEE Transactions on Biomedical Engineering. 2004; 51(6):881–9. [PubMed: 15188854]

54. Abidian MR, Martin DC. Multifunctional nanobiomaterials for neural interfaces. Advanced Functional Materials. 2009; 19(4):573–85.

55. Kipke DR, Shain W, Buzsaki G, Fetz E, Henderson JM, Hetke JF, et al. Advanced neurotechnologies for chronic neural interfaces: New horizons and clinical opportunities. Journal of Neuroscience. 2008 Nov 12; 28(46):11830–8. [PubMed: 19005048]

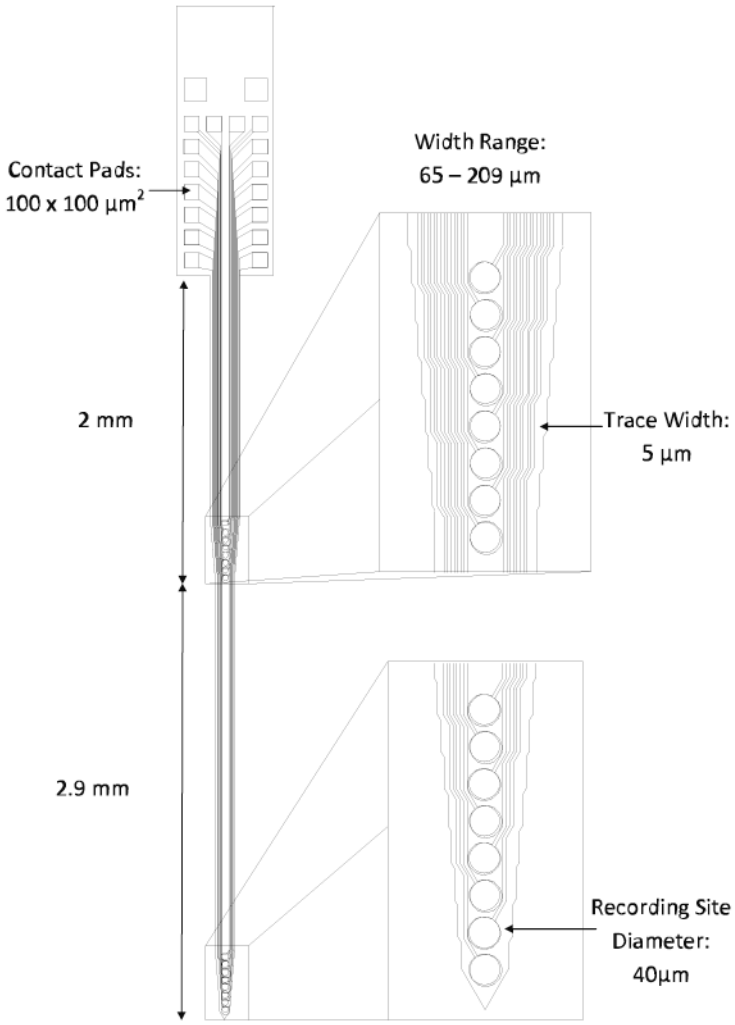

Figure 1.
Schematic representation of a titanium-based microfabricated microelectrode device designed for simultaneous acute recording in rat auditory cortex and thalamus.

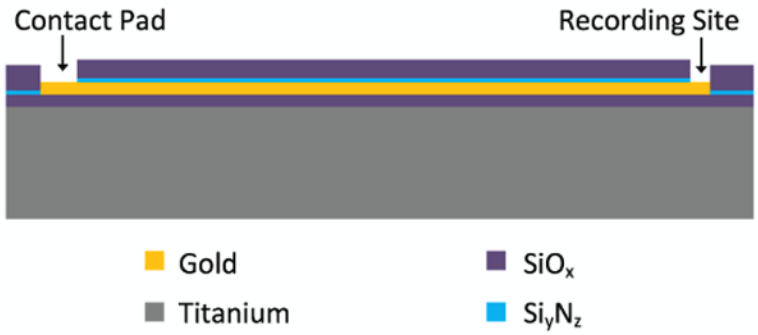

Figure 2.
Cross-sectional schematic of a single trace fabricated within a titanium-based microelectrode.

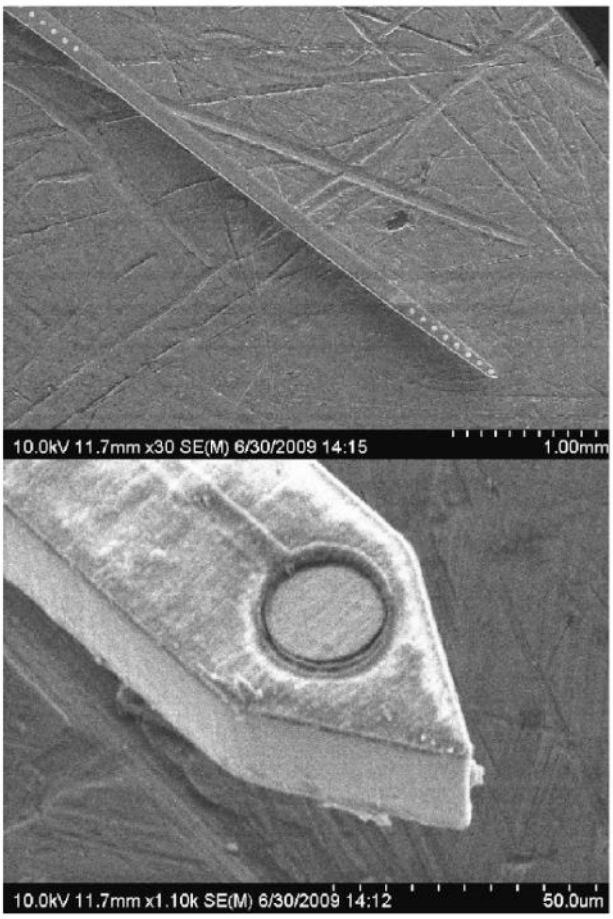

Figure 3.
Scanning electron micrographs of a titanium-based microelectrode.

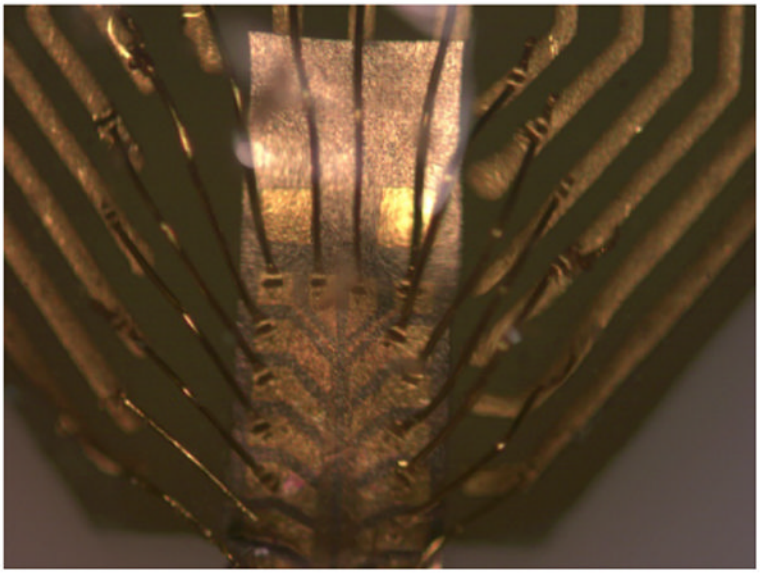

Figure 4. Titanium microelectrode gold wire-bonded to a PCB

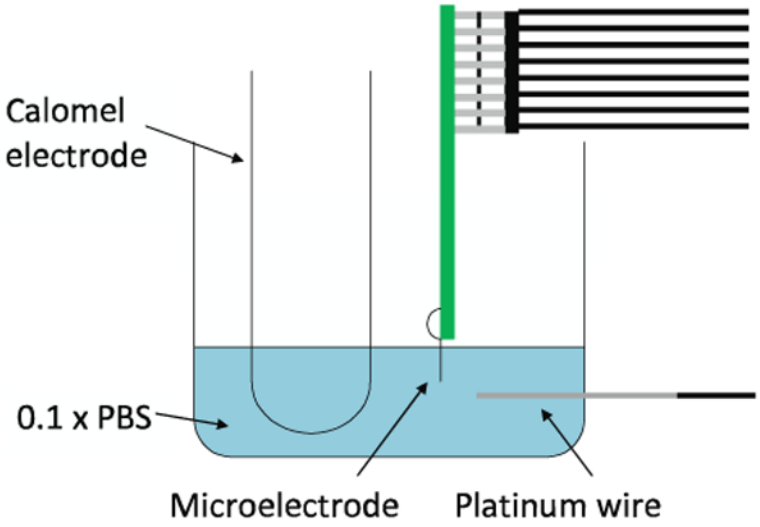

Figure 5.
In vitro testing apparatus.

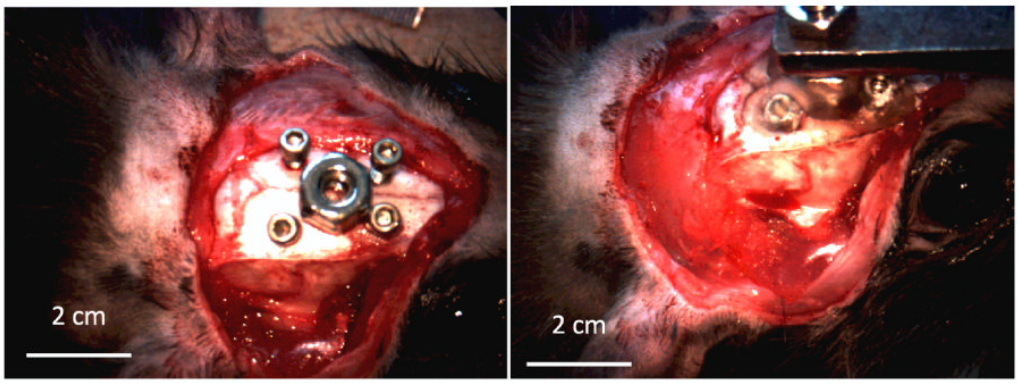

Figure 6.
Surgical head holder mounting.

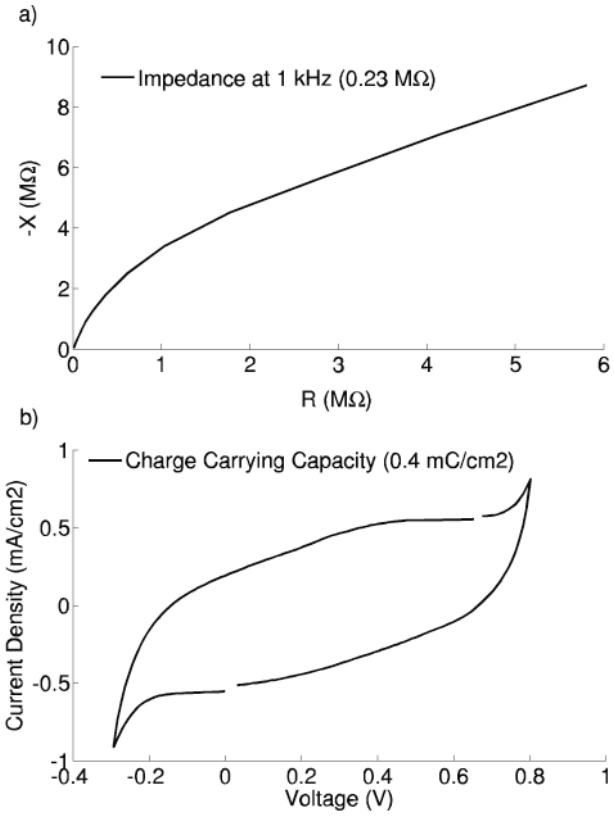

Figure 7.
a) EIS and b) CV plots for a 40 μm recording site from a 5.4 mm length titanium-based microelectrode.

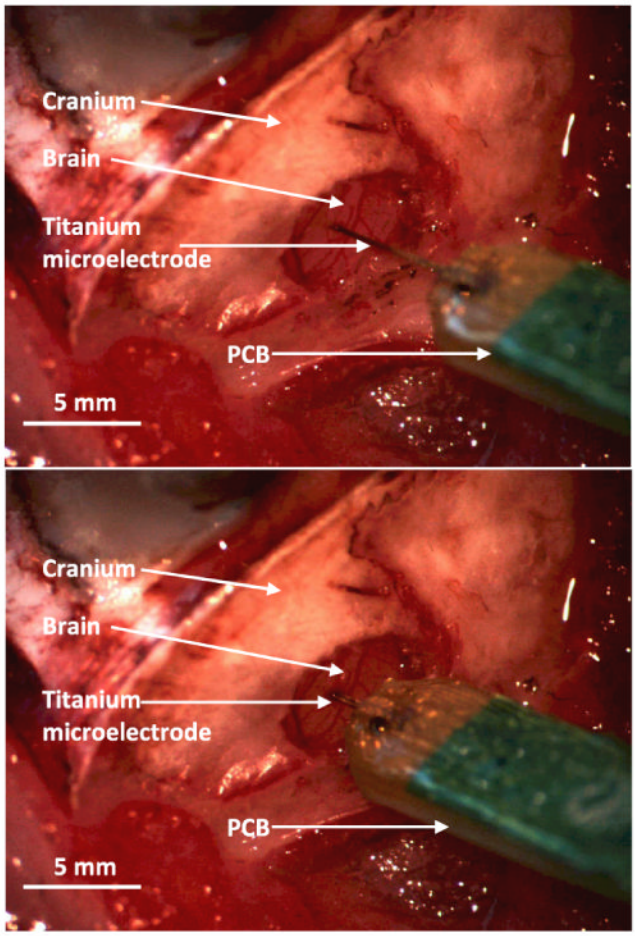

Figure 8.
Image captures from video recording of a titanium-based microelectrode insertion (through intact dura matter) into the auditory cortex.

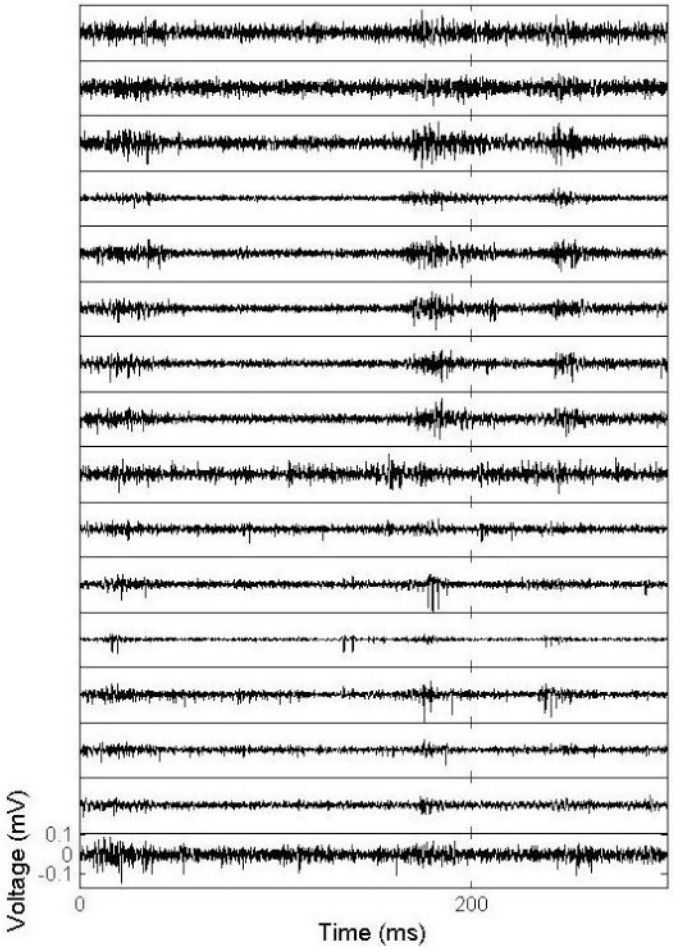

Figure 9.
Extracellular recordings from the auditory thalamus (bottom 8 traces) and auditory cortex (top 8 traces) of an anesthetized rat.

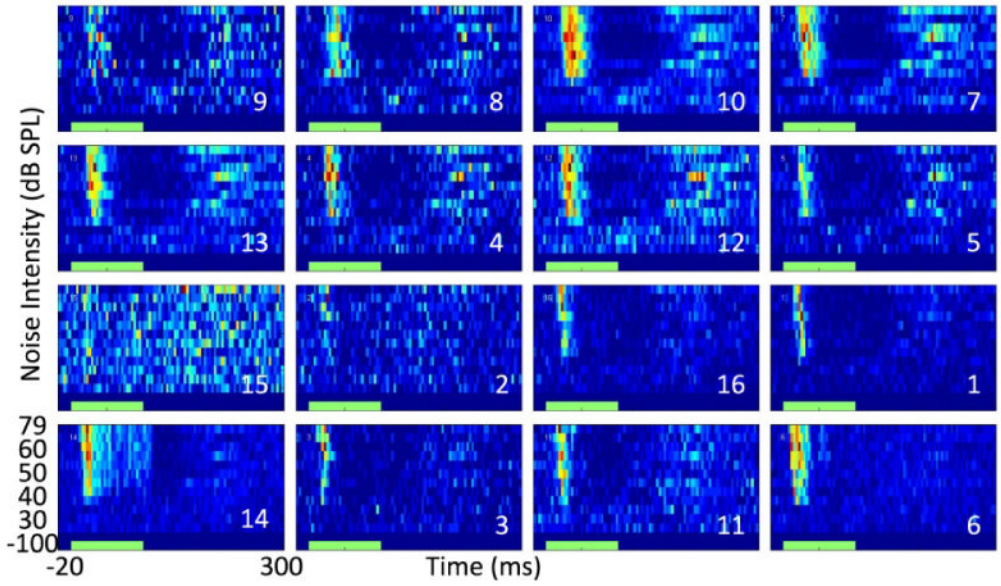

Figure 10.
Simultaneously-recorded, noise-evoked, peri-stimulus time histograms from the auditory cortex (top 2 rows) and thalamus (bottom 2 rows) of an anesthetized rat. The green bar along the x-axis reflects the timing of the broadband acoustic noise stimulus.

Table 1

Action potential recordings.

	Min	Max	Mean	Standard Deviation
Amplitude (mV)	62.87	432.55	173.91	109.79
Noise (mV)	16.89	39.83	31.93	6.18
Signal to Noise Ratio	3.09	13.05	5.23	3.05
Units	0	2	0.81	0.75
Total Units: 13				